

Early- and Late-Time Modifications to Λ CDM: Implications for the Hubble Tension

Rahul Dhyani,^{1,*} Purba Mukherjee,^{2,3,†} Arindam Chatterjee,^{1,‡} and Anjan A Sen^{2,§}

¹*Shiv Nadar Institution of Eminence (Deemed to be University),
Tehsil Dadri, Gautam Buddha Nagar, Uttar Pradesh 201314, India*

²*Centre for Theoretical Physics, Jamia Millia Islamia, New Delhi 110025, India*

³*Korea Astronomy and Space Science Institute (KASI), Daejeon 34055, Republic of Korea*

(Dated: May 26, 2026)

We investigate an extension of Λ CDM in which a fraction of cold Dark Matter (DM) decays into invisible dark radiation (DR) around the radiation–matter equality epoch, together with a non-standard dark energy (DE) equation of state characterized by w_0 . The decaying DM component modifies the early expansion history and reduces the sound horizon at baryon drag, while the DE alters the expansion rate at the late times. A comprehensive analysis combining Planck 2018+ACT DR6+DESI DR2+CMB lensing datasets has been carried out to explore the viability of this framework in addressing the H_0 tension. This model yields a Hubble constant of $H_0 = 69.83 \pm 0.98 \text{ km s}^{-1} \text{ Mpc}^{-1}$, reducing the discrepancy with SH0ES measurement to $\sim 2.2\sigma$ and local distance network measurement (H0DN) to $\sim 2.9\sigma$. Further, considering SH0ES and Pantheon+, the inferred value of the Hubble constant becomes $H_0 = 70.20 \pm 0.66 \text{ km s}^{-1} \text{ Mpc}^{-1}$. The Bayesian evidence suggests that this framework offers a fit to the relevant cosmological datasets at a statistically similar level as Λ CDM. It is observed that correlated early- and late-time modifications to the cosmological expansion history provide a more effective route to reducing the H_0 tension than either class of modification alone.

* rd947@snu.edu.in

† pdf.pukherjee@jmi.ac.in

‡ arindam.chatterjee@smu.edu.in

§ aasen@jmi.ac.in

I. INTRODUCTION

The simplest incarnation of the standard model of cosmology, Λ CDM, where Λ and CDM stand for cosmological constant and Cold Dark Matter, respectively, has been successful in light of a wide range of cosmological observations. These include observations probing the early and late stages of the evolution of our Universe, notably the Cosmic Microwave Background Radiation (CMBR) anisotropies [1, 2], as well as the large-scale structure (LSS) mapped by modern galaxy surveys[3–9]. Despite its remarkable success, increasing observational precision has revealed persistent tensions among independent cosmological probes. The most prominent among these are the discrepancies between early- and late-Universe determinations of the Hubble constant H_0 [1, 2, 10] and the amplitude of matter clustering inferred from weak-lensing and galaxy surveys compared to the CMB predictions, commonly expressed as the S_8 tension [11, 12]. In particular, the discrepancy in the H_0 , is significant and persists at the $(5 - 7)\sigma$ level [1, 2, 7, 8, 10, 13, 14], see also, e.g., [15–17]. Further, while results from the KiDS Legacy Survey indicate that the previously reported S_8 tension is no longer significant [18], recent DES-Y6 [19] results find that the tension persists at $\sim 2.8\sigma$ [9].

From the CMBR observations, assuming Λ CDM, Planck collaboration obtains $H_0 = 67.4 \pm 0.5 \text{ km s}^{-1} \text{ Mpc}^{-1}$ [1], while combining Planck and Atacama Cosmology Telescope (ACT) observations $H_0 = 67.64 \pm 0.5 \text{ km s}^{-1} \text{ Mpc}^{-1}$ [20]. The local distance ladder measurement of H_0 via Cepheid-calibrated SNIa from SHOES yields $H_0 = 73.04 \pm 1.04 \text{ km s}^{-1} \text{ Mpc}^{-1}$ [10]. The Local Distance Network (HODN) collaboration has reported a local measurement of the Hubble constant combining multiple independent distance indicators, and obtains $H_0 = 73.50 \pm 0.81, \text{ km, s}^{-1}, \text{ Mpc}^{-1}$ [14]. The estimation of H_0 differs from the joint Planck+SPT-3G+ACT (DR6) constraint at the level of 7.1σ [21], and from the Planck+ACT (DR6)+DESI(BAO) DR2 combination at approximately 6σ . Such a persistent and high-significance disagreement, termed as the Hubble tension, has attracted substantial attention in the literature [22–26].

The proposed resolutions may be broadly classified as follows. The first category includes modifications within the standard cosmological framework which alter processes, such as the reionization history [27, 28] or recombination¹[30–34]. The second category involves modification of the dark sector and/or the gravity sector beyond the simplest realization by introducing new degrees of freedom, novel interactions, and/or dynamics, modifying the evolution of the early Universe [26, 35–70]. Such scenarios aim to reconcile early- and late-time determinations of H_0 by altering the pre- or post-recombination dynamics, while remaining consistent with other cosmological observations. Further, various systematic uncertainties have been explored as possible sources [71–73].

It has been noted that an increase in H_0 without modifying the (comoving) sound horizon at baryon drag r_{drag} leads to tensions with BAO and Hubble parameter estimations from

¹ In this context, it may be noted that as compared to the Planck CMB determination $\tau_{\text{reio}} = 0.0544 \pm 0.0073$ [1], recent results based on JWST observations indicate a higher reionization optical depth, possibly reaching $\tau_{\text{reio}} \gtrsim 0.07$ [29].

type-Ia supernovae measurements, as the (comoving) angular diameter distance ($D(z)$) scales inversely with H_0 . As BAO measurements tightly constrain the combination $r_{\text{drag}}/D(z)$, therefore, extensions of Λ CDM which only affect the evolution of the Universe at late times has been less successful in resolving the Hubble tension. Further, as the sound horizon $r_{\text{drag}} = \int_{z_d}^{\infty} \frac{c_s(z)}{H(z)} dz$ scales inversely with the Hubble parameter $H(z)$, an increase in the early expansion rate $H(z)$ due to the additional energy component leads to a decrease in r_{drag} [74, 75].²

The present study considers an amalgamation of the early-time and late-time modifications of the evolution of the Universe. In particular, it incorporates a decaying fraction of DM, parametrized by f_{dcdm} , with a decay width Γ_{dcdm} , such that $\Gamma_{\text{dcdm}}^{-1} \simeq H_{EQ}$, where H_{EQ} denotes the Hubble parameter at the radiation–matter equality epoch and the subscript “dcdm” stands for decaying DM. For the late-time modification, the Dark Energy (DE) equation of state parameter w_0 , has been introduced. Further, the Chevallier–Polarski–Linder (CPL) parametrization with $w(a) = w_0 + w_a(1 - a)$, where (w_0, w_a) are the model parameters [76, 77] has also been considered.

Each of these extensions of Λ CDM have been widely studied in the literature. In particular, in the context of decaying DM, two possibilities have been considered in the literature: a one-parameter extension characterized solely by the decay rate Γ_{dcdm} , and a two-parameter extension in which a fraction f_{dcdm} of the CDM decays with rate Γ_{dcdm} into (relativistic) dark radiation (DR) and/or into warm dark matter (WDM) [78–93]. The resolution of the H_0 tension depends on the lifetime, given by the inverse of the decay width ($\Gamma_{\text{dcdm}}^{-1}$), and on the fraction of decaying DM (f_{dcdm}). Such a decay process in the early Universe leads to modifications in both the background energy densities and the evolution of cosmological perturbations. As for modifications of the DE equation of state, this is generally parameterized either by a constant value, $w = w_0$, or by a time-varying function $w(a)$, which, in Chevallier–Polarski–Linder (CPL) parametrization takes the following form $w(a) = w_0 + w_a(1 - a)$, where (w_0, w_a) are the model parameters [76, 77]. Such parametrizations can provide an effective phenomenological description of physical DE models [94] and successfully reproduce the observable signatures of quintessence scenarios [95]. It has been suggested that, while each of these extensions individually leads to an increase in H_0 to around $H_0 \simeq 69 \text{ km s}^{-1} \text{ Mpc}^{-1}$, these generally fall short of fully resolving the tension [74, 96]. This motivates the approach explored in this article, where fractional DCDM with $\Gamma_{\text{dcdm}}^{-1} \simeq H_{EQ}$ together with modification of the equation of state for DE has been considered. In light of recent cosmological observations from ACT DR6 [20] and DESI DR2 [97], in addition to Planck [1], SHOES [10] and Pantheon+ [98] a comprehensive analysis has been performed to explore the viability of this framework in addressing the H_0 tension.

² For example, Early Dark Energy (EDE) models, in which a scalar field temporarily contributes a non-negligible fraction of the total energy density before the recombination epoch and then rapidly dilutes, thereby increasing $H(z)$ at early times without significantly affecting late-time cosmology. BAO measurements tightly constrain the combination $r_{\text{drag}}/D(z)$, and a smaller r_{drag} requires corresponding shifts in distance measures that are not always favored by low-redshift data [41, 56, 61].

This paper is organized as follows. In Sec. II, we present the theoretical framework, describing the fractional decaying cold dark matter (f DCDM) sector and DE Parametrization. Our main results, including parameter constraints, posterior distributions, impacts on the Hubble constant H_0 tension, and comparisons with Λ CDM, are presented and discussed in Sec. III. Finally, Sec. IV provides a summary of the key findings, discusses implications for cosmology, and outlines directions for future work.

II. THE FRAMEWORK

In this section, we describe the extended cosmological framework that is considered for the present study. The base Λ CDM, has been extended to include three additional parameters in the CDM and DE sectors. In the CDM sector, it is assumed that a fraction f_{dcdm} of the total CDM abundance decays into invisible dark radiation with a decay width Γ_{dcdm} . For DE, the equation of state has been parametrized to account for non-trivial evolution of the respective energy density.

The combination of these two sectors allows correlated adjustments to early- and late-universe observables, offering a more flexible extension of Λ CDM than either modification allows for in isolation.

A. Fractional Decaying Cold Dark Matter (f DCDM)

In the present case, we consider a fraction of the DM which decays into invisible relativistic species (denoted as DCDM), hereafter referred to as dark radiation (DR) [80, 81, 85, 99, 100]. The decay is characterized by a constant decay width Γ_{dcdm} . The fractional abundance of the decaying component at a time $t_i \ll \Gamma_{\text{dcdm}}^{-1}$ in the cosmic comoving frame is denoted by f_{dcdm} , with the remaining fraction $(1 - f_{\text{dcdm}})$ consists of stable and non-interacting CDM (dubbed as SCDM). Since the decay produces DR, there are no constraints from electromagnetic energy injection and CMB spectral distortions. Thus, for $t \ll 1/\Gamma_{\text{dcdm}}$ the entire CDM abundance comprises of DCDM and SCDM, while for $t \gg 1/\Gamma_{\text{dcdm}}$ only SCDM contributes to the DM energy density. In the following discussion, this CDM sector will be referred to as f DCDM.

The decay process leads to energy transfer from DM to DR. The total energy-momentum tensor $T_{\text{T}}^{\mu\nu} = T_{\text{dr}}^{\mu\nu} + T_{\text{dcdm}}^{\mu\nu}$, where the subscripts dr and dcdm stand for contributions from DR and DCDM components, respectively, is covariantly conserved, i.e. $\nabla_{\mu} T_{\text{T}}^{\mu\nu} = 0$. Further, for $T_{\text{dr}}^{\mu\nu}$, $T_{\text{dcdm}}^{\mu\nu}$, we have,

$$\nabla_{\mu} T_{\text{dcdm}}^{\mu\nu} = -Q^{\nu}, \quad \nabla_{\mu} T_{\text{dr}}^{\mu\nu} = Q^{\nu}, \quad (1)$$

where the effect of the energy-momentum transfer from DCDM to DR is described by the

four-vector Q^ν as follows,

$$Q^\nu = a\Gamma_{\text{dcdm}}\rho_{\text{dcdm}}u_{\text{dcdm}}^\nu, \quad (2)$$

with u_{dcdm}^ν denoting the four-velocity of the DCDM fluid. The number of DCDM particles decaying per unit volume per unit comoving time is proportional to the decay width multiplied by the respective number density. Consequently, the rate of energy transfer per unit volume (in the comoving frame) to DR because of DCDM decay is proportional to this number density particles multiplied by the rest mass of the DCDM, and thus, $\Gamma_{\text{dcdm}}\rho_{\text{dcdm}}$. The four-velocity of DCDM (u_{dcdm}^ν) in the comoving frame, which is also the rest-frame of DCDM (i.e., $u_{\text{dcdm}}^0 = 1$), ensures the covariance of the above equation. This choice corresponds to decay in the rest frame of the parent particle. The resulting evolution equations for the background energy densities of DCDM (ρ_{dcdm}) and DR (ρ_{dr}) are

$$\rho'_{\text{dcdm}} + 3\mathcal{H}\rho_{\text{dcdm}} = -a\Gamma_{\text{dcdm}}\rho_{\text{dcdm}}, \quad (3)$$

$$\rho'_{\text{dr}} + 4\mathcal{H}\rho_{\text{dr}} = +a\Gamma_{\text{dcdm}}\rho_{\text{dcdm}}, \quad (4)$$

where prime denotes derivative with respect to conformal time, $\mathcal{H} \equiv a'/a$ is the conformal Hubble parameter, and a is the scale factor.

As described in Sec.I, f DCDM framework is parameterized by the initial fractional abundance f_{dcdm} , and the decay width Γ_{dcdm} of the DCDM. The first parameter is defined as the relative abundance of DCDM, and is given by,

$$f_{\text{dcdm}} = \frac{\rho_{\text{dcdm}}(t_i)}{\rho_{\text{dcdm}}(t_i) + \rho_{\text{scdm}}(t_i)} = \frac{\Omega_{\text{dcdm}}(t_i)}{\Omega_{\text{dcdm}}(t_i) + \Omega_{\text{scdm}}(t_i)}, \quad (5)$$

where $\Omega_{\text{cdm}} \equiv \Omega_{\text{dcdm}}(t_i) + \Omega_{\text{scdm}}(t_i)$ is the total CDM contribution. By construction, $f_{\text{dcdm}} \in [0, 1]$, with $f_{\text{dcdm}} = 0$ corresponding to the standard Λ CDM scenario, and $f_{\text{dcdm}} = 1$ corresponding to the case in which the entire CDM abundance is unstable.

The conversion of CDM into DR has several consequences, which depend on the timescale $\Gamma_{\text{dcdm}}^{-1}$. At $t \simeq \Gamma_{\text{dcdm}}^{-1}$, $\rho_{\text{dr}}(t)$ increases, leading to a small increment of the sound speed c_s in the same epoch. However, a larger matter abundance (in comparison with radiation) for $t > \Gamma_{\text{dcdm}}^{-1}$ leads to an enhancement in the Hubble parameter $H(z)$ at the corresponding redshifts z , and, therefore, the integral $\int_z^\infty \frac{c_s}{H(z)} dz$ decreases. This reduces the length scale for baryon drag r_{drag} . As discussed earlier, as BAO measurements constrain the ratio $r_{\text{drag}}/D(z)$, for $z \simeq z_d$, r_{drag} can be (slightly) reduced in this scenario. As $D \propto 1/H_0$, this ensures that BAO observations remain consistent with a large H_0 . The depletion of CDM can be consistent with an enhanced late-time expansion rate shifts the inferred Hubble constant H_0 toward higher values when fitting cosmological data, offering a pathway to reduce the Hubble tension. Finally, the additional DR modifies the late Integrated Sachs–Wolfe (ISW)

effect and CMB lensing, providing observational constraints on the f DCDM. Further, the enhancement of radiation leads to depletion in the growth of density perturbations, especially at small length scales. However, for $\Gamma_{\text{dcdm}} \simeq H_{EQ}$, this is negligible.³

Beyond the background evolution, the decay into DR alters the evolution of cosmological perturbations through explicit energy–momentum transfer between the DCDM component and DR. An analysis of the evolution of the density and velocity perturbations of various species is, therefore, essential for reliable estimations of CMB anisotropies and large-scale structure observables. We adopt the synchronous-gauge formulation for DCDM, following Ref.[100], where a single additional parameter Γ_{dcdm} was considered. This framework has been extended by including the fractional abundance of DCDM (f_{dcdm}) [80, 99]. We adopt the synchronous gauge and follow the notations of Ref. [102]. The perturbation equations governing the evolution of the density contrast δ_{dcdm} and velocity divergence θ_{dcdm} of the DCDM components are given by,

$$\delta'_{\text{dcdm}} = -\theta_{\text{dcdm}} - \frac{1}{2}h', \quad (6)$$

$$\theta'_{\text{dcdm}} = -\mathcal{H}\theta_{\text{dcdm}}. \quad (7)$$

In the above equation, h' denotes the derivative of the scalar perturbation in the synchronous gauge. Note that, in the synchronous gauge the perturbation equations for DCDM are unaffected by the decay term. As the CDM perturbations constitute equal-time hypersurface, and DCDM and CDM are both at rest in the comoving frame, thus, the decay of DM affects the background density, and the density contrast of DCDM in the same way leading to cancellation in the ratio δ_{dcdm} . The effect of the decay term, which, for example, appears in the Newtonian gauge, depletes the density contrast δ_{dcdm} [99]. The Euler equation for DCDM remains unchanged, as decay process does not affect the velocity divergencies.

The relativistic decay products contribute as DR. The perturbation equations governing the evolution of the lowest-order moments, including the density contrast δ_{dr} , velocity divergence θ_{dr} , and shear stress σ_{dr} , are given by

$$\delta'_{\text{dr}} = -\frac{2}{3}h' + a\Gamma_{\text{dcdm}}\frac{\rho_{\text{dcdm}}}{\rho_{\text{dr}}}(\delta_{\text{dcdm}} - \delta_{\text{dr}}), \quad (8)$$

$$\theta'_{\text{dr}} = k^2\left(\frac{1}{4}\delta_{\text{dr}} - \sigma_{\text{dr}}\right) - a\Gamma_{\text{dcdm}}\frac{\rho_{\text{dcdm}}}{\rho_{\text{dr}}}\theta_{\text{dcdm}}, \quad (9)$$

$$\sigma'_{\text{dr}} = \frac{4}{15}\theta_{\text{dr}} - \frac{3}{5}kF_{\text{dr},3} - \frac{2}{15}h' - \frac{1}{5}\eta' - a\Gamma_{\text{dcdm}}\frac{\rho_{\text{dcdm}}}{\rho_{\text{dr}}}\sigma_{\text{dr}}, \quad (10)$$

where η is the traceless scalar metric perturbation in the synchronous gauge, and $F_{\text{dr},3}$ is the $\ell = 3$ multipole moment of the perturbed DR distribution function. The decay-induced source

³ In contrast, decays at much later times primarily suppress clustering without substantially altering r_{drag} [101].

terms for DR signifies the transfer of energy and momentum at the level of perturbation. The higher-order multipoles ($\ell \geq 3$) evolve according to the standard Boltzmann hierarchy for massless particles. As mentioned, at the very early times $\mathcal{H} \gg \Gamma_{\text{dcdm}} a$, the probability of decay is negligible. Thus, in the CDM sector, the initial conditions are set by the standard adiabatic initial conditions of Λ CDM. In this regime, the perturbations of the DCDM component are indistinguishable from those of SCDM, while DR perturbations are initially suppressed. On the contrary, for $\Gamma_{\text{dcdm}} \gg \frac{\mathcal{H}}{a}$, the CDM comprises of SCDM, as most of DCDM would have decayed around $\Gamma_{\text{dcdm}} \simeq \frac{\mathcal{H}}{a}$. In the present context, the priors on the parameter Γ_{dcdm} ensures that the range of $\Gamma_{\text{dcdm}}^{-1}$ includes the radiation–matter equality epoch.

B. Dark Energy Parameterization

Within the standard Λ CDM framework, the accelerated expansion of the Universe [103] is attributed to a cosmological constant Λ , characterized by a time-independent equation of state $w = -1$. This simplest empirical framework, while consistent with current observational data, raises several concerns, most notably the well-known cosmological constant problem and the coincidence problem [104, 105]. These shortcomings have motivated extensive investigations into dynamical DE models [106], potentially offering a more satisfactory description of the accelerated expansion.

In this context, a natural and widely adopted approach is to parameterize the DE equation-of-state parameter, defined as $w(a) \equiv p_{\text{de}}/\rho_{\text{de}}$, where p_{de} and ρ_{de} are the pressure and energy density of the DE, respectively. Such phenomenological parameterizations allow for a model-independent estimation of possible deviations from a cosmological constant in a systematic and unbiased manner. In the present context, we adopt the following parameterization,

$$w(a) = w_0, \quad (11)$$

where w_0 is a free parameter, and does not vary with time. This corresponds to a one-parameter extension in the DE sector, as compared to the Λ CDM. It is worth mentioning that $w_0 = -1$ reproduces the cosmological constant, the DE density scales as $\rho_{\text{de}} \propto a^{-3(1+\omega_0)}$. The regime $w_0 > -1$ describes quintessence-like behavior, in which the DE density decreases with time, whereas $w_0 < -1$ corresponds to the phantom regime, associated with a DE density that grows with the expansion of the Universe [106–113]. The latter scenario violates the null energy condition, potentially signaling the need for exotic physics beyond standard scalar field models [110]. Despite its simplicity, this one-parameter extension provides a valuable first test of deviations from Λ CDM and serves as a useful baseline. In this article, we also comment on a two-parameter extended DE sector, the Chevallier–Polarski–Linder

(CPL) parameterization [76, 77], which introduces a linear dependence on the scale factor a ,

$$w(a) = w_0 + w_a (1 - a), \quad (12)$$

where w_0 is the present-day value of the equation of state and w_a quantifies the rate of its dynamical evolution. At the present epoch ($a = 1$), this expression reduces to $w = w_0$, while at early times ($a \rightarrow 0$) it asymptotes to a finite value $w_0 + w_a$. The respective DE density scales as, $\rho_{\text{de}}(a) \propto a^{-3(1+w_0+w_a)} \exp[-3 w_a (1 - a)]$. This reduces to the Λ CDM result for $w_0 = -1$ and $w_a = 0$. These DE modifications are implemented at the level of the background expansion history and are subsequently combined with the two-parameter ($f_{\text{dcdm}}, \Gamma_{\text{dcdm}}$) extension of CDM sector described in Sec. II A, with the goal of constructing a comprehensive and physically motivated framework for addressing the H_0 tension from both the early- and late-time sides simultaneously.

III. RESULTS

TABLE I: Flat prior ranges adopted for the parameters that extend the baseline Λ CDM model. The prior on $\log_{10}(\Gamma_{\text{dcdm}})$ is chosen to ensure that decays occur around or before radiation-matter equality.

Parameter	Symbol	Prior range
Decay rate (log)	$\log_{10}(\Gamma_{\text{dcdm}}/\text{km s}^{-1} \text{Mpc}^{-1})$	[5.5, 8.5]
Decaying DM fraction	f_{dcdm}	[0, 0.2]
DE EoS	w_0	[-3.0, 1.0]
DE EoS slope	w_a	[-3.0, 2.0]

In this section, we present the observational constraints on the extensions of the standard model of cosmology, as described in Sec. II in light of cosmological data. In particular, we discuss the implications on the CMB anisotropies, the matter power spectrum, and on the cosmological tensions. Broadly, we analyze the following scenarios:

1. **Model-A** : Fractional DCDM (f DCDM) (with $w_0 = -1$)

A fraction f_{dcdm} of cold dark matter decays into invisible DR with a constant decay width Γ_{dcdm} , with no free parameter in the DE sector (i.e., cosmological constant).

2. **Model-B** : Fractional DCDM (f DCDM) + evolving DE

The same decaying dark matter component is combined with a constant equation of state w_0 for DE. Also, we briefly touch upon the implications for the CPL parametrization (w_0, w_a).

TABLE II: Cosmological datasets used in this analysis.

Sl. no.	Dataset	Likelihood component	Multipole range / Redshift
1	Planck 2018 [1]	Low- ℓ TT	$\ell = 2-29$
		Low- ℓ EE (Sroll12)	$\ell = 2-29$
		High- ℓ TT (ACT cut)	$\ell \leq 1000$
		High- ℓ TE/EE	$\ell \leq 600$
2	ACT DR6 [114]	High- ℓ TT/TE/EE	$\ell \gtrsim 600$
3	CMB lensing	CMB lensing reconstruction	$\ell \leq 4000$
4	DESI DR2 [8]	BAO distance measurements	All redshift bins
5	SHOES + Pantheon+ [98]	Cepheid distance ladder	$0 < z \lesssim 2.3$
		+ SN Ia magnitude	

Parameter inference is performed through a Bayesian Markov Chain Monte Carlo (MCMC) analysis using the publicly available package COBAYA [115] interfaced with the publicly available Boltzmann equation solver CLASS [116] where the covariant Λ CDM perturbation equations were implemented. The code was modified extending the analysis to the fractional-decaying DM, as described in Ref. [100]. We vary the six baseline Λ CDM parameters $\{\Omega_b h^2, \Omega_{\text{cdm}} h^2, 100\theta_{\text{MC}}, \tau_{\text{reio}}, \log(10^{10} A_s), n_s\}$ together with the model-specific parameters $f_{\text{dcdm}}, \log_{10}(\Gamma_{\text{dcdm}}/\text{km s}^{-1} \text{Mpc}^{-1})$ and w_0 . Further, w_a is also varied while considering CPL parameterization for DE sector. The parameters considered, and the respective flat priors have been mentioned in Table I. The combination of datasets used is detailed in Table II. For early times, datasets 1-4 have been used. While for late times, dataset 5 has been added. In this set, Pantheon+ supernovae data have been used with Cepheid calibration from SHOES. We have used SHOES data in this context, as it provides robust calibration in the entire low redshift range. Further, H_0 obtained by SHOES and HODN are very similar [10, 14]. To assess the convergence of the chains, the Gelman–Rubin criterion $R - 1 < 0.01$ [117, 118] has been followed. For model comparison, the difference in best-fit χ^2 , $\Delta\chi^2 \equiv \chi^2_{\text{model}} - \chi^2_{\Lambda\text{CDM}}$, has been used, where negative values favour the extended model.

A. Implications on the Parameters in the Dark Sector

In the following, we discuss the extended Dark Sector models discussed above in light of the cosmological data, as mentioned in Table II.

a. Model-A [f DCDM benchmark (with $w_0 = -1$)]: We first consider the simplest extension of Λ CDM, among the models considered in this study, i.e., with f DCDM. As mentioned earlier, it is referred to as Model-A. The equation of state for DE is fixed at $w_0 = -1$. For the analysis, data sets 1 to 4, as mentioned in Table II have been used. The

TABLE III: Mean values and 1σ uncertainties of cosmological parameters obtained from the combined Planck 2018 + ACT DR6 + DESI DR2 (BAO) data. The quantity $\Delta\chi^2 \equiv \chi_{\text{model}}^2 - \chi_{\Lambda\text{CDM}}^2$ is computed with respect to the baseline ΛCDM model. Upper limits on f_{dcdm} and Σm_ν are at 95% CL.

Parameter	ΛCDM	Model-A	Model-B	Model-B+ Σm_ν
$A_s \times 10^9$	2.10 ± 0.03	2.147 ± 0.026	2.135 ± 0.026	2.136 ± 0.025
n_s	0.974 ± 0.003	0.9797 ± 0.0048	0.9775 ± 0.0049	0.9781 ± 0.0046
$100\theta_s$	1.0411 ± 0.0003	1.0419 ± 0.0003	1.0419 ± 0.0003	1.04186 ± 0.00026
$\Omega_b h^2$	0.0224 ± 0.00015	0.02251 ± 0.00012	0.02249 ± 0.00012	0.02250 ± 0.00012
$\Omega_{\text{cdm}} h^2$	0.120 ± 0.001	0.1217 ± 0.0034	0.1222 ± 0.0033	0.1226 ± 0.0032
τ_{reio}	0.0624 ± 0.007	0.0635 ± 0.0064	0.0615 ± 0.0069	0.0613 ± 0.0062
w_0	-1 (fixed)	-1 (fixed)	-1.035 ± 0.036	-1.025 ± 0.038
f_{dcdm}	-	< 0.064	< 0.062	< 0.061
$\log_{10}\left(\frac{\Gamma_{\text{dcdm}}}{\text{km s}^{-1} \text{Mpc}^{-1}}\right)$	-	7.72 ± 0.52	7.75 ± 0.50	7.72 ± 0.54
Σm_ν [eV]	0.06 (fixed)	0.06 (fixed)	0.06 (fixed)	< 0.10
H_0	68.38 ± 0.28	68.98 ± 0.47	69.83 ± 0.98	69.70 ± 0.99
S_8	0.817 ± 0.007	0.823 ± 0.014	0.824 ± 0.014	0.834 ± 0.013
$\Omega_\Lambda(\Omega_{fld})$	0.690 ± 0.04	0.6951 ± 0.0053	0.7059 ± 0.0073	0.7053 ± 0.0074
r_{drag} [Mpc]	147.58 ± 0.20	146.98 ± 0.45	146.88 ± 0.45	146.88 ± 0.44
$\Delta\chi^2$	0	-2.90	-3.60	-5.2

TABLE IV: Mean values and 1σ uncertainties obtained from the combined Planck+ACT+DESI DR2+SHOES+Pantheon+ dataset.

Parameter	Planck+ACT+DESI DR2+SHOES+Pantheon+	
	ΛCDM	Model-B
$\log(10^{10} A_s)$	3.051 ± 0.012	3.050 ± 0.011
n_s	0.9762 ± 0.0031	0.9875 ± 0.0050
$100\theta_s$	1.04187 ± 0.00024	1.04213 ± 0.00025
$\Omega_b h^2$	0.022617 ± 0.000107	0.022549 ± 0.000113
$\Omega_{\text{cdm}} h^2$	0.11690 ± 0.00062	0.13019 ± 0.00317
τ_{reio}	0.0659 ± 0.0064	0.0623 ± 0.0059
w_0	-1 (fixed)	-1.025 ± 0.021
w_a	—	—
f_{dcdm}	-	0.073 ± 0.017
$\log_{10}(\Gamma_{\text{dcdm}}/\text{km s}^{-1} \text{Mpc}^{-1})$	-	7.85 ± 0.25
H_0 [$\text{km s}^{-1} \text{Mpc}^{-1}$]	68.60 ± 0.26	70.20 ± 0.66
S_8	0.807 ± 0.007	0.828 ± 0.010
r_{drag} [Mpc]	147.66 ± 0.19	146.45 ± 0.50
$\Delta\chi^2$	0	-8.8

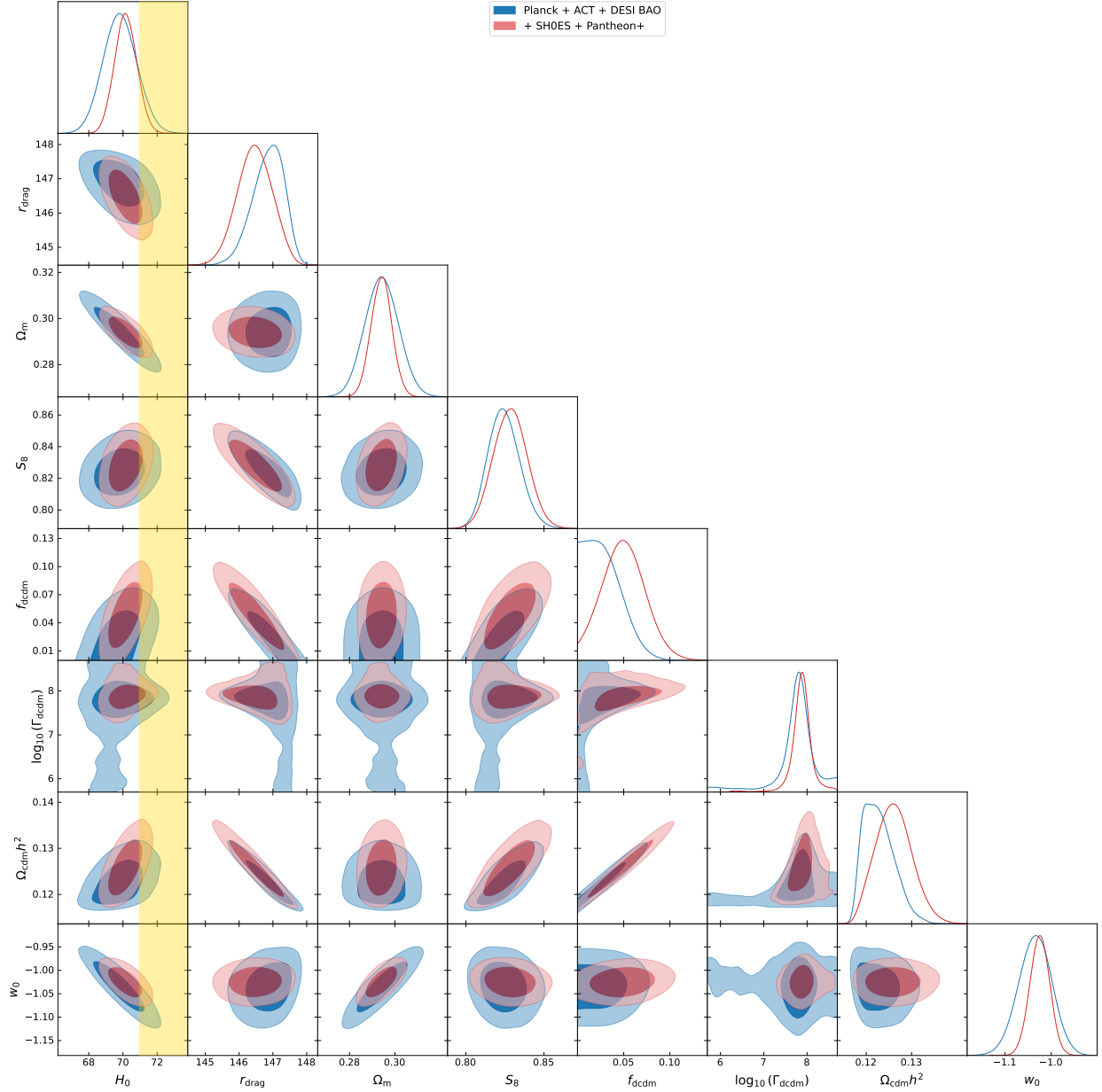


FIG. 1: Triangle plot for Model-B showing the marginalized posterior distributions for the parameters ω_{cdm} , Ω_m , $\log \Gamma_{\text{dcdm}}$ (log decay rate), S_8 , H_0 , r_{drag} (sound horizon at drag epoch), f_{dcdm} (fraction of decaying dark matter), and w_0 (dark energy equation-of-state parameter). The **blue** contours correspond to the dataset combination Planck +ACT DR(6)+DESI BAO (DR2), while the **red** contours correspond to Planck + ACT (DR6)+DESI BAO (DR2) +SHOES+Pantheon+. All panels display both the 1σ (68%,C.L.) and 2σ (95%,C.L.) confidence regions. The **gold shaded band** represents the 2σ SHOES constraint on H_0 .

best fit values, and the allowed range of the parameters have been mentioned in the second column of Table III.

The best fit value for Γ_{dcdm} is given by $\Gamma_{\text{dcdm}} = 5.25 \times 10^7 \text{ km s}^{-1} \text{ Mpc}^{-1}$, and the parameter lies approximately between $1.5 \times 10^7 - 1.8 \times 10^8 \text{ km s}^{-1} \text{ Mpc}^{-1}$ at 68% c.l. while the decaying

fraction is constrained as $f_{\text{dcdm}} < 0.064$ (at 95% c.l.). The Hubble parameter today (H_0) shifts upward to $H_0 = 68.98 \pm 0.47 \text{ km s}^{-1} \text{ Mpc}^{-1}$, reducing the discrepancy with the HODN measurement [14] from approximately 6.0σ to 4.8σ . The best fit value of Γ_{dcdm} corresponds to a lifetime of the decaying component of approximately $\mathcal{O}(10^4)$ years, which is well after the Big Bang Nucleosynthesis (BBN) epoch, and around the radiation–matter equality epoch. The sound horizon at baryon drag is mildly compressed to $r_{\text{drag}} = 146.98 \pm 0.45 \text{ Mpc}$, approximately 0.6 Mpc below the ΛCDM value, in accordance with the discussion in Sec. II.

In the following, we comment on the BBN constraints in this context. The success of BBN imposes constraints on the Hubble parameter, and consequently, the number of relativistic species (with the same temperature as the SM plasma) [119, 120]. However, for $f_{\text{dcdm}} \simeq 0.06$, around $z \simeq 10^9$ (temperature $T \simeq \mathcal{O}(1 - 10) \text{ MeV}$) the relative change in the Hubble parameter during BBN is given by $\left. \frac{H^{f_{\text{DCDM}}}-H^{\Lambda\text{CDM}}}{H^{\Lambda\text{CDM}}} \right|_{(T \simeq 1 \text{ MeV})} \ll 0.001$. This is because, during BBN DCDM behaves as matter, and as it contributes less than 10% of the CDM, its contribution to the expansion rate at $T \simeq 1 \text{ MeV}$, which falls in the radiation-dominated epoch, remains insignificant. For the same reason, there is no contribution to the effective number of additional relativistic species ΔN_{eff} at the onset of BBN in this scenario. It is also worth noting that, as the decay width of the DCDM component is very small, the respective interaction strength of DCDM and DR is negligibly small, and thus, in the early Universe DCDM and DR components would not be in thermal equilibrium in this scenario. This is in contrast to the models described in Refs. [121–123], where CDM–DR interactions are appreciable in the early Universe. However, the stability of CDM is typically ensured by underlying symmetry principles, and no decaying component is present. Thus, appreciable production of the DR component does not happen before the BBN epoch in this scenario. However, as the DCDM decays to DR around the radiation-matter equality epoch, it produces additional radiation. Consequently, the energy density in the radiation bath increases. As the decay process happens towards the end of the radiation-dominated epoch, $f_{\text{dcdm}} \lesssim 10\%$ implies that the contribution from the DCDM to the total energy density is less than 5% approximately. Consequently, at the epoch of recombination, which is in the matter-dominated epoch, the respective relativistic decay products contribute less than 1.5%, as the radiation energy density depletes by a factor of a^{-1} faster compared to the matter density. Therefore, the constraint on ΔN_{eff} (< 0.15 at recombination) from ACT is respected for the 95% upper limit on f_{dcdm} , as depicted in Table III. The sum of the (three species of) neutrino masses Σm_ν is set to 0.06 eV for the present analysis.

b. Model-B [$w_0 + f_{\text{DCDM}}$ model]: Introducing a constant DE equation of state alongside the f_{DCDM} component yields a more pronounced improvement, as far as the Hubble tension is concerned. As depicted in Table III, with datasets 1-4 (see Table II), there is a mild but statistically non-zero preference for a decaying fraction f_{dcdm} ,

$$f_{\text{dcdm}} = 0.027 \pm 0.019 \quad (< 0.062 \text{ at } 95\% \text{ C.L.}). \quad (13)$$

The best-fit value for the decay width Γ_{dcdm} such that the life-time $\Gamma_{\text{dcdm}}^{-1}$ of the DCDM particle is around the radiation–matter equality epoch, and is given by,

$$\log_{10}\left(\frac{\Gamma_{\text{dcdm}}}{\text{km s}^{-1} \text{Mpc}^{-1}}\right) = 7.75 \pm 0.50. \quad (14)$$

In this scenario, for the r_{drag} is reduced by a further ~ 0.1 Mpc relative to the best fit point **Model-A**. The Hubble parameter in the present epoch is increased to, $H_0 = 69.83 \pm 0.98 \text{ km s}^{-1} \text{Mpc}^{-1}$.

This shows a significant upward shift as compared to its value in Λ CDM, as well from **Model-A**, reducing the residual tension with the HODN local measurement [14] to $\sim 2.9\sigma$. The inferred equation of state of DE is given by $w_0 = -1.035 \pm 0.036$, is consistent with a cosmological constant at the 1σ level. It displays a marginal phantom preference that provides additional late-time expansion without any significant effect on the CMB acoustic peaks. The matter clustering amplitude remains essentially unaffected, $S_8 = 0.829 \pm 0.014$, which is consistent with large-scale structure observations. The overall goodness of fit improved compared to Λ CDM ($\Delta\chi^2 \approx -3.6$). This suggests that the upward shift in H_0 arises from early- and late-time effects, providing a better fit to both CMBR and BAO. The value of H_0 obtained in this framework is in good agreement with the SH0ES measurement and is within less than 2.5σ , significantly reducing the tension of H_0 . Consequently, in addition to the datasets 1-4 in Table II, we considered the SH0ES + Pantheon+, as mentioned in the fifth row of the same table. This further enhances the Hubble parameter in the present epoch $H_0 = 70.20 \pm 0.66; \text{km s}^{-1} \text{Mpc}^{-1}$, raising the central value and reducing the uncertainty. The parameter r_{drag} is decreased to 146.45 Mpc. All the relevant parameters have been shown in Table VII. This improvement is primarily due to the preference of the late-time datasets to a higher expansion rate. The goodness of fit improved compared to Λ CDM ($\Delta\chi^2 \approx -8.8$). It is worth noting that, as shown in Figure.1, the posteriors of the decay width Γ_{dcdm} show clear peaks for both **Model-A** and **Model-B**, demonstrating a preference for the decaying component around the epoch of radiation-matter equality epoch. The $2\text{-}\sigma$ contours include the entire prior range, while considering datasets sensitive to the early universe i.e., CMB (including lensing) and BAO (serial no. 1–4 in Table. II). This is because the prior range in f_{dcdm} includes zero, and Γ_{dcdm} becomes unconstrained as $f_{\text{dcdm}} \rightarrow 0$. The contours for f_{dcdm} change substantially after including the datasets SH0ES+PantheonPlus (serial no. 5 in Table.II) which include the measurement of H_0 via Cepheid-calibrated Supernova-type IA and are sensitive to the late Universe. In this case, $f_{\text{dcdm}} \rightarrow 0$ becomes disfavored at $1\text{-}\sigma$, and consequently, the contours for Γ_{dcdm} is well constrained around the best-fit values. Note that, for a given f_{dcdm} a very large Γ_{dcdm} corresponds to a smaller lifetime of DCDM, and thus, it decays well within the radiation-dominated epoch, producing DR. Consequently, the effect $H(z)$ and, thus, on r_{drag} is not substantial. For much smaller Γ_{dcdm} , the decay takes place around the recombination epoch, which is disfavored by CMBR. Note that, as expected,

f_{dcdm} shows a positive correlation with H_0 , and a negative correlation with r_{drag} . Note that, as mentioned earlier, including SHOES+ Pantheon+(mentioned in sl.no 5 in Table.II); substantially raises H_0 and one obtains $H_0 = 70.20$. The details have been mentioned in Table. IV.

Next, we comment on the implications on the sum of the neutrino masses Σm_ν in this context. For our analysis, as mentioned in the third column of Table III, Σm_ν is set to 0.06 eV. As this parameter is correlated with w_0 [124, 125], therefore, an extension of Model-B varying Σm_ν has also been considered. The results have been stated in the fourth column of Table III. The upper limit on Σm_ν is relaxed to 0.1 eV.⁴ There is an increase in the decay width Γ_{dcdm} by about a factor of 1.5, as compared to the scenario, where Σm_ν was fixed at 0.06 eV. No significant change in the upper limit of f_{dcdm} is noticed. Note that an early decay of the DCDM component would correspond to further depletion of the DR, as compared to matter density around the recombination epoch. It (partially) contributes to a proportionate increase in the upper limit of Σm_ν , enhancing the contribution of the (semi-)relativistic neutrino species around the same epoch. Note that this increase in the upper limit to 0.1eV (at 95% c.l.) allows the inverted hierarchy in the neutrino sector to remain a viable possibility.

To evaluate the statistical viability of the models beyond goodness-of-fit metrics, we perform a Bayesian model comparison utilizing the PolyChord nested sampling algorithm [126]. The computed log-Bayes factors yield strictly $|\ln B| < 1$ (+0.48), denoting an inconclusive statistical preference on the empirical Jeffreys scale. Furthermore, while the incorporation of late-time observational datasets precipitates a marginal posterior shift favouring the extended Model-B cosmology (-0.9), this enhanced phenomenological fit only partially mitigates the inherent Occam penalty exacted by the introduction of additional model parameters.⁵

Finally, we briefly comment on the extension of Model-B, with evolving DE equation of state described by the Chevallier–Polarski–Linder (CPL) parametrization as $w(z) = w_0 + w_a(1 - a)$. Using the datasets 1-4 in Table II, we obtain $H_0 = 65.4 \pm 2.52 \text{ km s}^{-1} \text{ Mpc}^{-1}$. There is substantial broadening of the H_0 posterior as compared to Model-A which likely reflects a degeneracy between w_a and the early-time decay parameters. We will not explore this possibility further in this article.

B. Status of H_0 (and S_8) Tension in the Extended Models

As the focus of the present study is to address the cosmological tensions, in the following, we present a discussion on the status of the tensions in the extended dark sector frameworks.

⁴ In appendix A, Table VI, a one parameter extension of Λ CDM with Σm_ν , and a two parameter extension with w_0 , Σm_ν have been depicted for a reference. The relaxation of the (68%) upper limit of Σm_ν is maximal for Model-B.

⁵ The detailed χ^2 contributions for the respective datasets, along with the results of the Bayesian analysis, are presented in Table VII and will be discussed subsequently.

TABLE V: Constraints on the Hubble constant H_0 for **Model-B** from the combination of **Planck+ACT (DR6)+DESI(BAO) DR2** data in various cosmological models, along with the residual tension with respect to the local measurement from the **HODN Collaboration [14]**,

$$H_0 = 73.50 \pm 0.81 \text{ km s}^{-1} \text{ Mpc}^{-1}, \text{ and the } \text{SHOES Collaboration [10]}, \\ H_0 = 73.04 \pm 1.04 \text{ km s}^{-1} \text{ Mpc}^{-1}. \text{ Tensions are quoted in units of } \sigma \text{ significance.}$$

Model	H_0 [km s ⁻¹ Mpc ⁻¹]	HODN tension	SHOES tension
Λ CDM	68.38 ± 0.28	$\sim 6.0 \sigma$	$\sim 4.3 \sigma$
Model-A	68.98 ± 0.47	$\sim 4.8 \sigma$	$\sim 3.4 \sigma$
w_0 CDM	69.11 ± 1.00	$\sim 3.4 \sigma$	$\sim 2.8 \sigma$
Model-B	69.83 ± 0.98	$\sim 2.9 \sigma$	$\sim 2.2 \sigma$

Figure 2 shows the marginalized posterior distributions of H_0 for the Λ CDM baseline and the $w_0 + f$ DCDM hybrid model, compared against the local distance-ladder measurements from **SHOES [10]** and **HODN [14]**. The Λ CDM fit to **Planck+ACT (DR6)+DESI(BAO) DR2** data, i.e., serial no. 1-4 in Table II, yields

$$H_0^{\Lambda\text{CDM}} = 68.38 \pm 0.28 \text{ km s}^{-1} \text{ Mpc}^{-1} \quad (68\% \text{ C.L.}), \quad (15)$$

in tension with the local distance-ladder measurements at the $\sim 6.0\sigma$ level. In **Model-B**, the H_0 posterior shifts towards higher values,

$$H_0^{\text{Model-B}} = 69.83 \pm 0.98 \text{ km s}^{-1} \text{ Mpc}^{-1} \quad (68\% \text{ C.L.}), \quad (16)$$

reducing the tension with the local measurements to $\sim 2.9\sigma$, can be seen in Figure 2. This shift is driven by the interplay between the DCDM component, parametrized by the decay rate Γ_{dcdm} and DCDM fraction f_{dcdm} , and the DE equation-of-state parameter w_0 , which together modify the late-time expansion history in a manner that partially alleviates the H_0 discrepancy.

Table V summarises the Hubble constant posterior for all the models considered in this work, using the combined dataset **Planck+ACT (DR6)+DESI(BAO) DR2**, i.e., serial no. 1-4, as mentioned in Table II. The successive extensions of the dark sector shift the inferred values progressively upward: introducing **Model-A** raises H_0 to $68.98 \pm 0.47 \text{ km s}^{-1} \text{ Mpc}^{-1}$, reducing the tension to $\sim 4.8 \sigma$; allowing a constant DE equation of state w_0 without f DCDM gives $H_0 = 69.11 \pm 1.00 \text{ km s}^{-1} \text{ Mpc}^{-1}$ ($\sim 3.4 \sigma$); and the combination of both — the **Model-B** — yields the largest shift, $H_0 = 69.83 \pm 0.98 \text{ km s}^{-1} \text{ Mpc}^{-1}$, lowering the residual tension to $\sim 2.9 \sigma$. With the addition of **SHOES** and **Pantheon+** data, as shown in Table IV), **Model-B** yields $H_0 = 70.20 \pm 0.66 \text{ km s}^{-1} \text{ Mpc}^{-1}$, significantly closer to local distance-ladder measurements.

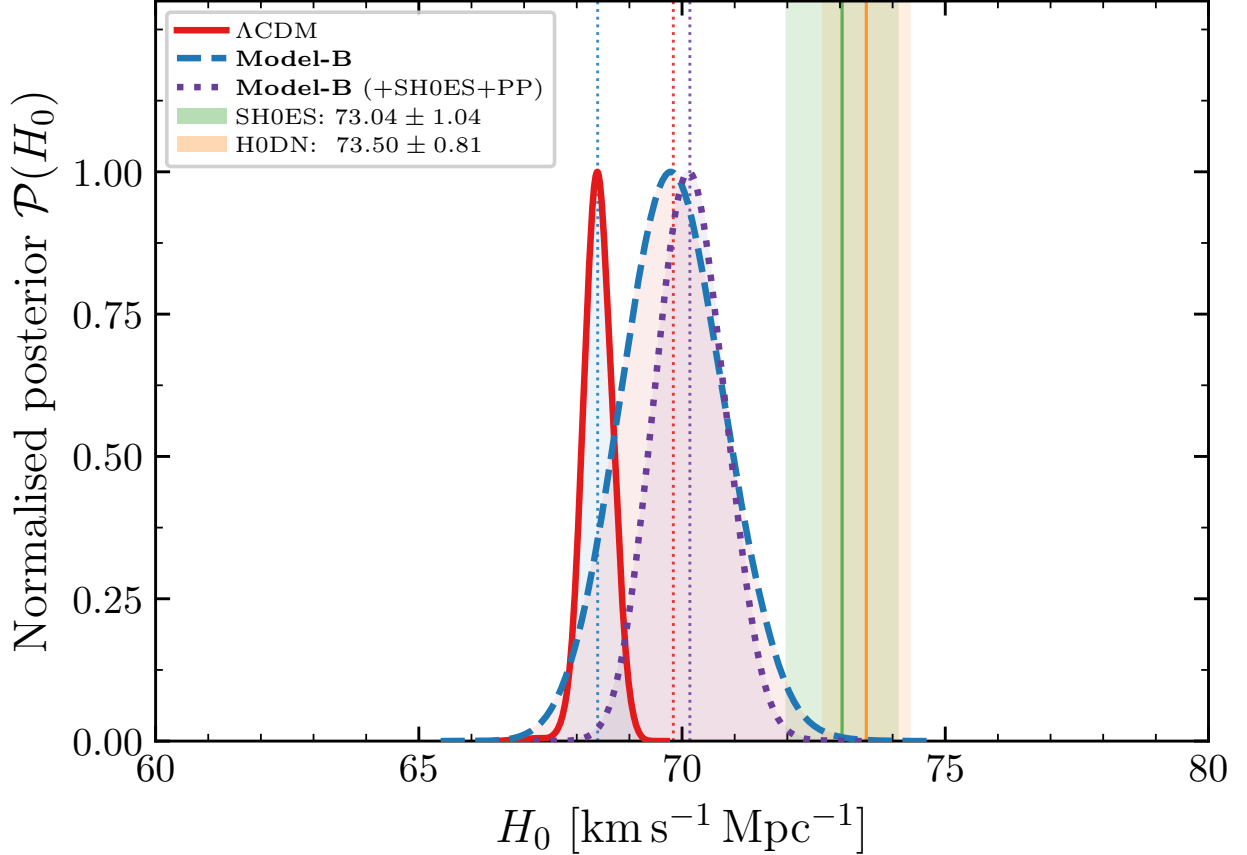


FIG. 2: Marginalized posterior distributions of H_0 for the Λ CDM baseline (solid red), **Model-B** (dashed blue), and **Model-B + SH0ES (SH0ES+PP)** (dotted purple), where **PP** refers to **Pantheon+**. The Λ CDM and Model-B constraints are obtained using Planck + ACT DR6 + DESI DR2, while the purple curve additionally includes the SH0ES with Pantheon+. Shaded vertical bands indicate the local distance-ladder measurements from SH0ES $73.04 \pm 1.04 \text{ km s}^{-1} \text{ Mpc}^{-1}$ [10] and HODN $73.50 \pm 0.81 \text{ km s}^{-1} \text{ Mpc}^{-1}$ [14]. Thin dotted vertical lines mark the posterior mean values for each model.

The progressive improvement in H_0 follows directly from the physical mechanisms described in Sec. II: DM decays near radiation–matter equality compress r_{drag} , while DE amplifies the late-time expansion. This is illustrated in Figure 3. The left panel shows a negative correlation between H_0 and r_{drag} in **Model-B**, and a bigger parameter region favoured by the data. The right panel demonstrates H_0 vs Ω_m in **Model-B**, where a larger region is favoured by the data

Next, we comment on the S_8 tension in the context of the extended models considered in this work. The S_8 values inferred across all models remain in mild tension with weak-lensing measurements from surveys such as KiDS and DES, which typically report $S_8 \sim 0.76\text{--}0.78$ [9], while results from the KiDS Legacy Survey indicate that the previously reported S_8 tension is no longer significant [18]. The f DCDM models yield slightly higher $S_8 \approx 0.828\text{--}0.829$ compared to Λ CDM ($S_8 = 0.817$). The introduction of DCDM alone does not fully alleviate

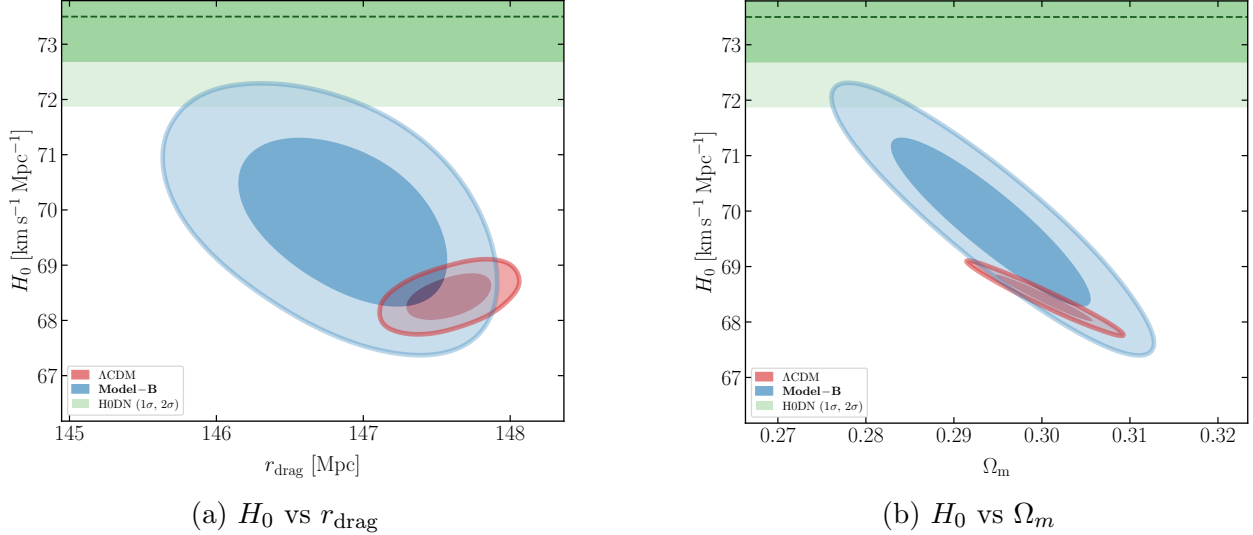


FIG. 3: 2D marginalized contours (68% and 95% C.L.) in Λ CDM (red) and Model-B (blue) with a H0DN $(1 - 2\sigma)$ on H_0 [14]. *Left:* H_0 vs sound horizon at baryon drag r_{drag} . *Right:* H_0 vs present-day matter density parameter Ω_m .

this tension. However, interactions between the residual SCDM and baryons with an effective cross-section (σ_{dmeff}) can suppress small-scale power sufficiently to ease the S_8 tension [127, 128]. To illustrate, we have considered SCDM with a mass of 0.1 MeV, which gives a S_8 central value of around 0.817. In this case, the tension with the H0DN measurement of H_0 is reduced to 2.8σ . Further details, including the best fit values in the model, are given in the Table. VI in Appendix A.

Finally, it is worth briefly commenting on how these models compare with extended frameworks, such as EDE and relevant extended versions in light of cosmological data. An updated analysis of EDE variants has recently appeared in Ref. [129]. The improved H_0 in Model-B yields $H_0 = 69.83 \pm 0.98 \text{ km s}^{-1} \text{Mpc}^{-1}$ for the Planck + ACT DR6 + DESI DR2 dataset combination, increasing to $H_0 = 70.20 \pm 0.66 \text{ km s}^{-1} \text{Mpc}^{-1}$ after including SH0ES+Pantheon+. These values are comparable to recent axion-like EDE analyses, where single-field EDE models typically prefer $H_0 \sim 69.71 \text{ km s}^{-1} \text{Mpc}^{-1}$ [129], as obtained considering similar datasets. In two and three field EDE scenarios H_0 can increase further to $\sim 70.5\text{--}70.9 \text{ km s}^{-1} \text{Mpc}^{-1}$ [130] with Planck 2018 Commander + SimAll + Lensing(PR3) + CamSpec PR4 + PantheonPlus + DESI DR2 datasets. Therefore, the behaviour of Model-B is broadly comparable with such resolutions of the Hubble tension. Also, recently, in Ref. [131] an EDE scenario combined with a late-time thawing DE model has been studied. Their inferred value of H_0 is consistent with the result obtained from Model-B in our analysis.

IV. CONCLUSION

In this article, a cosmological scenario is presented extending the Λ CDM with fractional DCDM (f DCDM) and a DE component with an equation of state parameterized by w_0 . The f DCDM component decays to massless DR species around the radiation–matter equality epoch. A comprehensive Bayesian MCMC analysis has been performed using Planck 2018 TT/TE/EE, ACT DR6, DESI DR2 BAO, Planck CMB lensing, and SHOES+Pantheon+ to estimate the relevant parameters. The important findings include the following.

- **Model-A** increases the Hubble constant to $H_0 = 68.98 \pm 0.47 \text{ km s}^{-1} \text{ Mpc}^{-1}$ (68% C.L.) by reducing r_{drag} through f DCDM decay around radiation–matter equality, accommodating a higher CMB-inferred H_0 . **Model-B**, which additionally includes the DE equation-of-state parameter w_0 , further raises it to $H_0 = 69.83 \pm 0.98 \text{ km s}^{-1} \text{ Mpc}^{-1}$ (68% C.L.), reducing the tension with SHOES to 2.2σ and with HODN to 2.9σ . **Model-B** also provides an improved fit over Λ CDM with $\Delta\chi^2 = -8.8$ (full dataset), while remaining comparably favored under Bayesian model comparison.
- The DE equation-of-state parameter (w_0) in **Model-B** marginally enters the phantom region. However, $w_0 = -1$ remains allowed at 1σ .
- We observe that the constraint on f_{dcdm} remains nearly unchanged for both **Model-A** and **Model-B** when considering the PLANCK+ACT (DR2)+lensing+DESI BAO (DR2) dataset (serial no.1-4 in table. II). However, upon adding the SHOES+Pantheon+ (serial no.5-6 in table. II) data, a non-zero central value for f_{dcdm} is obtained, with a preference for non-zero f_{dcdm} emerging at the 1σ level.
- We also analyze an extension of **Model-B** including the summed neutrino mass parameter, $\sum m_\nu$. In this case, the upper bound on $\sum m_\nu$ weakens to 0.10 eV (95% C.L.), compared to upper limit on the Λ CDM+ $\sum m_\nu$ bound of 0.068 eV . Consequently, the model relaxes the neutrino mass constraints sufficiently to allow the possibility of an inverted neutrino mass hierarchy.
- BBN and CMB constraints on ΔN_{eff} are satisfied throughout the parameter space. For $f_{\text{dcdm}} \lesssim 0.06$, the modification to the expansion rate during BBN is negligible, while the decay occurs near matter–radiation equality, leading to only mild effects on the CMB. It is also important to note that **Model-B** achieves an improvement in H_0 comparable to that obtained in other extensions, such as Early Dark Energy (EDE) models, using the latest cosmological data.
- The S_8 tension is not alleviated in **Model-B**; however, allowing the stable DM component (SCDM) to interact with electrons or protons can suppress small-scale power and reduce the S_8 tension, as illustrated.

TABLE VI: Mean values and 1σ uncertainties of cosmological parameters obtained from the combined Planck 2018 + ACT + DESI DR2 (BAO) data. The quantity $\Delta\chi^2 \equiv \chi_{\text{model}}^2 - \chi_{\Lambda\text{CDM}}^2$ is computed with respect to the baseline ΛCDM model. Upper limits on f_{dcdm} , σ_{dmeff} , and Σm_ν are at 95% CL.

Parameter	ΛCDM	$\Lambda\text{CDM} + \Sigma m_\nu$	$w_0\text{CDM}$	$w_0w_a\text{CDM}$	$w_0w_a + f\text{DCDM}$	DM- e Scattering
$A_s \times 10^9$	2.10 ± 0.03	2.130 ± 0.024	2.134 ± 0.025	2.11 ± 0.003	2.11 ± 0.002	2.134 ± 0.023
n_s	0.974 ± 0.003	0.9744 ± 0.0031	0.9744 ± 0.0034	0.971 ± 0.004	0.975 ± 0.004	0.9784 ± 0.0048
$100\theta_s$	1.0411 ± 0.0003	1.04179 ± 0.00025	1.04178 ± 0.00025	1.04169 ± 0.00025	1.04179 ± 0.00026	1.04199 ± 0.00031
$\Omega_b h^2$	0.0224 ± 0.00015	0.02254 ± 0.00010	0.02254 ± 0.00011	0.02248 ± 0.00011	0.02246 ± 0.00012	0.02250 ± 0.00012
$\Omega_{\text{cdm}} h^2$	0.120 ± 0.001	0.1178 ± 0.0006	0.1176 ± 0.0009	0.1190 ± 0.0011	0.1228 ± 0.0030	0.1220 ± 0.0034
τ_{reio}	0.0624 ± 0.007	0.0626 ± 0.0061	0.0609 ± 0.0063	0.059 ± 0.006	0.058 ± 0.006	0.0608 ± 0.0063
w_0	-1 (fixed)	-1 (fixed)	-1.025 ± 0.039	-0.48 ± 0.21	-0.58 ± 0.27	-1.028 ± 0.039
w_a	-	-	-	-1.54 ± 0.60	-1.2 ± 0.75	-
f_{dcdm}	-	-	-	-	< 0.056	< 0.059
$\log_{10}\left(\frac{\Gamma_{\text{dcdm}}}{\text{km s}^{-1} \text{Mpc}^{-1}}\right)$	-	-	-	-	7.83 ± 0.45	7.72 ± 0.52
$\sigma_{\text{dmeff}} [\text{cm}^2]$	-	-	-	-	-	$< 3.35 \times 10^{-27}$
$\Sigma m_\nu [\text{eV}]$	0.06 (fixed)	< 0.068	0.06 (fixed)	0.06 (fixed)	0.06 (fixed)	0.06 (fixed)S
H_0	68.38 ± 0.28	68.59 ± 0.29	69.11 ± 1.00	64.1 ± 1.9	65.4 ± 2.52	69.69 ± 1.09
$\Omega_\Lambda(\Omega_{\text{fld}})$	0.690 ± 0.04	0.7011 ± 0.0036	0.7049 ± 0.0081	0.715 ± 0.005	0.716 ± 0.008	0.705 ± 0.008
$r_{\text{drag}} [\text{Mpc}]$	147.58 ± 0.20	147.51 ± 0.19	147.31 ± 0.24	147.24 ± 0.26	146.77 ± 0.45	146.95 ± 0.48
S_8	0.817 ± 0.007	-	-	-	-	0.817 ± 0.015
$\Delta\chi^2$	0	-1.2	-0.5	-5.8	-10.1	-0.6

Upcoming surveys such as Euclid [132] and the Rubin Observatory LSST [133] will significantly improve constraints on extended dark-sector scenarios through precise measurements of large-scale structure and cosmic expansion. These observations may provide decisive tests of DCDM frameworks and help clarify the origin of the H_0 tension.

ACKNOWLEDGEMENTS

RD acknowledges CSIR, India for financial support through Senior Research Fellowship (File no. 09/ 1128 (13346)/ 2022 EMR-I) and Shiv Nadar IoE (Deemed to be University). AC acknowledges a helpful discussion with Subinoy Das. AAS acknowledges the funding from ANRF, Govt of India, under the research grant no. CRG/2023/003984. This article/publication is based upon work from COST Action CA21136- ‘‘Addressing observational tensions in cosmology with systematics and fundamental physics (CosmoVerse)’’, supported by COST (European Cooperation in Science and Technology). PM acknowledges funding from Anusandhan National Research Foundation (ANRF), Govt of India, Under the National Post-Doctoral Fellowship (File no. PDF/2023/001986).

Appendix A

The following table depicts various relevant extended models in light of Sl.no 1-4 from Table. II in Table. VI. The Bayesian evidence, together with χ^2 analyses for Model-B have

TABLE VII: Best-fit χ^2 values for Λ CDM and w_0+f DCDM for two dataset combinations. $\Delta\chi^2$ is computed with respect to Λ CDM; negative values indicate improvement. The Bayes factor $\ln \mathcal{B} = \ln(Z_{\Lambda\text{CDM}}/Z_{w_0+f\text{DCDM}})$. Dashes indicate datasets not included in a given combination.

Dataset	(i) Planck+ACT DR6 + DESI DR2			(ii) +SH0ES + Pantheon+		
	Λ CDM	Model-B	$\Delta\chi^2$	Λ CDM	Model-B	$\Delta\chi^2$
<i>CMB</i>						
Planck low- ℓ TT	21.72	21.57	-0.15	21.42	20.91	-0.51
Planck low- ℓ EE (scroll2)	391.47	390.27	-1.20	390.35	390.46	+0.11
ACT DR6 CMB (PlanckActCut)	221.19	221.98	+0.79	222.63	224.82	+2.19
ACT DR6 CMB	159.20	155.36	-3.84	160.92	155.52	-5.40
ACT DR6 Lensing	19.66	19.61	-0.05	20.18	19.92	-0.26
<i>Total CMB</i>	813.24	808.79	-4.45	815.48	811.61	-3.87
<i>Large-scale structure & distance</i>						
DESI BAO DR2	11.10	11.89	+0.79	10.33	11.10	+0.77
SH0ES+Pantheon+		—		1482.58	1476.91	-5.67
Total χ^2	824.34	820.68	-3.66	2308.42	2299.6268	-8.8
$\ln \mathcal{B}$			+0.48 \pm 0.07			-0.9 \pm 0.08

been presented in the Table. VII

-
- [1] Planck Collaboration, Planck 2018 results. vi. cosmological parameters, [Astron. Astrophys. **641**, A6 \(2020\)](#).
 - [2] E. Calabrese *et al.* (Atacama Cosmology Telescope), The Atacama Cosmology Telescope: DR6 constraints on extended cosmological models, [JCAP \(11\), 063, arXiv:2503.14454 \[astro-ph.CO\]](#).
 - [3] M. Betoule *et al.* (SDSS), Improved Cosmological Constraints from a Joint Analysis of the SDSS-II and SNLS Supernova Samples, [Astron. Astrophys. **568**, A22 \(2014\)](#), [arXiv:1401.4064 \[astro-ph.CO\]](#).
 - [4] S. Alam *et al.* (eBOSS), Completed SDSS-IV extended Baryon Oscillation Spectroscopic Survey: Cosmological implications from two decades of spectroscopic surveys at the Apache Point Observatory, [Phys. Rev. D **103**, 083533 \(2021\)](#), [arXiv:2007.08991 \[astro-ph.CO\]](#).

- [5] T. M. C. Abbott *et al.* (DES), The Dark Energy Survey: Cosmology Results with ~ 1500 New High-redshift Type Ia Supernovae Using the Full 5 yr Data Set, *Astrophys. J. Lett.* **973**, L14 (2024), [arXiv:2401.02929 \[astro-ph.CO\]](#).
- [6] A. G. Adame *et al.* (DESI), DESI 2024 III: baryon acoustic oscillations from galaxies and quasars, *JCAP* (04), 012, [arXiv:2404.03000 \[astro-ph.CO\]](#).
- [7] DESI Collaboration, Desi 2024 vi: Cosmological constraints from the measurements of baryon acoustic oscillations, *arXiv e-prints* (2024), [2404.03002](#).
- [8] K. Lodha *et al.* (DESI), Extended dark energy analysis using DESI DR2 BAO measurements, *Phys. Rev. D* **112**, 083511 (2025), [arXiv:2503.14743 \[astro-ph.CO\]](#).
- [9] T. M. C. Abbott *et al.* (DES), Dark Energy Survey Year 6 Results: Cosmological Constraints from Galaxy Clustering and Weak Lensing (2026), [arXiv:2601.14559 \[astro-ph.CO\]](#).
- [10] A. G. Riess *et al.*, A Comprehensive Measurement of the Local Value of the Hubble Constant with $1 \text{ km s}^{-1} \text{ Mpc}^{-1}$ Uncertainty from the Hubble Space Telescope and the SH0ES Team, *Astrophys. J. Lett.* **934**, L7 (2022), [arXiv:2112.04510 \[astro-ph.CO\]](#).
- [11] E. Di Valentino *et al.*, Cosmology Intertwined III: $f\sigma_8$ and S_8 , *Astropart. Phys.* **131**, 102604 (2021), [arXiv:2008.11285 \[astro-ph.CO\]](#).
- [12] I. Pantos and L. Perivolaropoulos, Status of the S_8 Tension: A 2026 Review of Probe Discrepancies (2026), [arXiv:2602.12238 \[astro-ph.CO\]](#).
- [13] L. Verde, N. Schöneberg, and H. Gil-Marín, A Tale of Many H_0 , *Ann. Rev. Astron. Astrophys.* **62**, 287 (2024), [arXiv:2311.13305 \[astro-ph.CO\]](#).
- [14] S. Casertano *et al.* (H0DN), The Local Distance Network: a community consensus report on the measurement of the Hubble constant at 1% precision, - (2025), [arXiv:2510.23823 \[astro-ph.CO\]](#).
- [15] L. Verde, T. Treu, and A. G. Riess, Tensions between the Early and the Late Universe, *Nature Astron.* **3**, 891 (2019), [arXiv:1907.10625 \[astro-ph.CO\]](#).
- [16] E. Di Valentino *et al.*, Snowmass2021 - Letter of interest cosmology intertwined II: The hubble constant tension, *Astropart. Phys.* **131**, 102605 (2021), [arXiv:2008.11284 \[astro-ph.CO\]](#).
- [17] L. Perivolaropoulos and F. Skara, Challenges for Λ CDM: An update, *New Astron. Rev.* **95**, 101659 (2022), [arXiv:2105.05208 \[astro-ph.CO\]](#).
- [18] B. Stözlner *et al.*, KiDS-Legacy: Consistency of cosmic shear measurements and joint cosmological constraints with external probes, *Astron. Astrophys.* **702**, A169 (2025), [arXiv:2503.19442](#)

- [astro-ph.CO].
- [19] T. M. C. Abbott *et al.* (DES), Dark Energy Survey Year 6 Results: Cosmological Constraints from Cosmic Shear (2026), [arXiv:2602.10065](#) [astro-ph.CO].
- [20] T. Louis *et al.* (Atacama Cosmology Telescope), The Atacama Cosmology Telescope: DR6 power spectra, likelihoods and Λ CDM parameters, *JCAP* (11), 062, [arXiv:2503.14452](#) [astro-ph.CO].
- [21] E. Camphuis *et al.* (SPT-3G), SPT-3G D1: CMB temperature and polarization power spectra and cosmology from 2019 and 2020 observations of the SPT-3G Main field, - (2025), [arXiv:2506.20707](#) [astro-ph.CO].
- [22] E. Di Valentino, A. Melchiorri, and J. Silk, Reconciling Planck with the local value of H_0 in extended parameter space, *Phys. Lett. B* **761**, 242 (2016), [arXiv:1606.00634](#) [astro-ph.CO].
- [23] T. Karwal and M. Kamionkowski, Dark energy at early times, the Hubble parameter, and the string axiverse, *Phys. Rev. D* **94**, 103523 (2016), [arXiv:1608.01309](#) [astro-ph.CO].
- [24] W. L. Freedman, Cosmology at a Crossroads, *Nature Astron.* **1**, 0121 (2017), [arXiv:1706.02739](#) [astro-ph.CO].
- [25] S. M. Feeney, D. J. Mortlock, and N. Dalmaso, Clarifying the Hubble constant tension with a Bayesian hierarchical model of the local distance ladder, *Mon. Not. Roy. Astron. Soc.* **476**, 3861 (2018), [arXiv:1707.00007](#) [astro-ph.CO].
- [26] E. Di Valentino, O. Mena, S. Pan, L. Visinelli, W. Yang, A. Melchiorri, D. F. Mota, A. G. Riess, and J. Silk, In the realm of the Hubble tension—a review of solutions, *Class. Quant. Grav.* **38**, 153001 (2021), [arXiv:2103.01183](#) [astro-ph.CO].
- [27] A. Chatterjee, T. R. Choudhury, and S. Mitra, CosmoReionMC: a package for estimating cosmological and astrophysical parameters using CMB, Lyman- α absorption, and global 21 cm data, *Mon. Not. Roy. Astron. Soc.* **507**, 2405 (2021), [arXiv:2101.11088](#) [astro-ph.CO].
- [28] I. J. Allali, P. Singh, J. Fan, and L. Li, Reionization and the Hubble constant: correlations in the Cosmic Microwave Background, *JCAP* (08), 082, [arXiv:2503.05691](#) [astro-ph.CO].
- [29] J. B. Muñoz, J. Mirocha, J. Chisholm, S. R. Furlanetto, and C. Mason, Reionization after JWST: a photon budget crisis?, *Mon. Not. Roy. Astron. Soc.* **535**, L37 (2024), [arXiv:2404.07250](#) [astro-ph.CO].
- [30] M. Liu, Z. Huang, X. Luo, H. Miao, N. K. Singh, and L. Huang, Can Non-standard Recombination Resolve the Hubble Tension?, *Sci. China Phys. Mech. Astron.* **63**, 290405 (2020),

- [arXiv:1912.00190 \[astro-ph.CO\]](#).
- [31] M. Rashkovetskiy, J. B. Muñoz, D. J. Eisenstein, and C. Dvorkin, Small-scale clumping at recombination and the Hubble tension, *Phys. Rev. D* **104**, 103517 (2021), [arXiv:2108.02747 \[astro-ph.CO\]](#).
- [32] S. H. Mirpoorian, K. Jedamzik, and L. Pogosian, Modified recombination and the Hubble tension, *Phys. Rev. D* **111**, 083519 (2025), [arXiv:2411.16678 \[astro-ph.CO\]](#).
- [33] G. P. Lynch, L. Knox, and J. Chluba, DESI observations and the Hubble tension in light of modified recombination, *Phys. Rev. D* **110**, 083538 (2024), [arXiv:2406.10202 \[astro-ph.CO\]](#).
- [34] K. Jedamzik, L. Pogosian, and T. Abel, Hints of primordial magnetic fields at recombination and implications for the Hubble tension, *Nature Astron.* **10**, 317 (2026), [arXiv:2503.09599 \[astro-ph.CO\]](#).
- [35] L. Zhang, X. Chen, M. Kamionkowski, Z.-g. Si, and Z. Zheng, Constraints on radiative dark-matter decay from the cosmic microwave background, *Phys. Rev. D* **76**, 061301 (2007), [arXiv:0704.2444 \[astro-ph\]](#).
- [36] A. Chudaykin, D. Gorbunov, and I. Tkachev, Dark matter component decaying after recombination: Lensing constraints with Planck data, *Phys. Rev. D* **94**, 023528 (2016), [arXiv:1602.08121 \[astro-ph.CO\]](#).
- [37] E. Di Valentino, A. Melchiorri, E. V. Linder, and J. Silk, Constraining Dark Energy Dynamics in Extended Parameter Space, *Phys. Rev. D* **96**, 023523 (2017), [arXiv:1704.00762 \[astro-ph.CO\]](#).
- [38] S. D. Odintsov, D. Sáez-Chillón Gómez, and G. S. Sharov, Is exponential gravity a viable description for the whole cosmological history?, *Eur. Phys. J. C* **77**, 862 (2017), [arXiv:1709.06800 \[gr-qc\]](#).
- [39] R. C. Nunes, Structure formation in $f(T)$ gravity and a solution for H_0 tension, *JCAP* (05), 052, [arXiv:1802.02281 \[gr-qc\]](#).
- [40] E. Mörtzell and S. Dhawan, Does the Hubble constant tension call for new physics?, *JCAP* (09), 025, [arXiv:1801.07260 \[astro-ph.CO\]](#).
- [41] V. Poulin, T. L. Smith, T. Karwal, and M. Kamionkowski, Early Dark Energy Can Resolve The Hubble Tension, *Phys. Rev. Lett.* **122**, 221301 (2019), [arXiv:1811.04083 \[astro-ph.CO\]](#).
- [42] S. D. Odintsov, D. Saez-Chillon Gomez, and G. S. Sharov, Testing logarithmic corrections on R^2 -exponential gravity by observational data, *Phys. Rev. D* **99**, 024003 (2019),

- [arXiv:1807.02163 \[gr-qc\]](#).
- [43] L. Knox and M. Millea, Hubble constant hunter’s guide, *Phys. Rev. D* **101**, 043533 (2020), [arXiv:1908.03663 \[astro-ph.CO\]](#).
- [44] K. L. Pandey, T. Karwal, and S. Das, Alleviating the H_0 and σ_8 anomalies with a decaying dark matter model, *JCAP* (07), 026, [arXiv:1902.10636 \[astro-ph.CO\]](#).
- [45] D. Wang and D. Mota, Can $f(T)$ gravity resolve the H_0 tension?, *Phys. Rev. D* **102**, 063530 (2020), [arXiv:2003.10095 \[astro-ph.CO\]](#).
- [46] M. Ballardini, M. Braglia, F. Finelli, D. Paoletti, A. A. Starobinsky, and C. Umiltà, Scalar-tensor theories of gravity, neutrino physics, and the H_0 tension, *JCAP* (10), 044, [arXiv:2004.14349 \[astro-ph.CO\]](#).
- [47] G. Ballesteros, A. Notari, and F. Rompineve, The H_0 tension: ΔG_N vs. ΔN_{eff} , *JCAP* (11), 024, [arXiv:2004.05049 \[astro-ph.CO\]](#).
- [48] M. Zumalacarregui, Gravity in the Era of Equality: Towards solutions to the Hubble problem without fine-tuned initial conditions, *Phys. Rev. D* **102**, 023523 (2020), [arXiv:2003.06396 \[astro-ph.CO\]](#).
- [49] S. J. Clark, K. Vattis, and S. M. Koushiappas, Cosmological constraints on late-universe decaying dark matter as a solution to the H_0 tension, *Phys. Rev. D* **103**, 043014 (2021), [arXiv:2006.03678 \[astro-ph.CO\]](#).
- [50] B. S. Haridasu and M. Viel, Late-time decaying dark matter: constraints and implications for the H_0 -tension, *Mon. Not. Roy. Astron. Soc.* **497**, 1757 (2020), [arXiv:2004.07709 \[astro-ph.CO\]](#).
- [51] D. Wang, Can $f(R)$ gravity relieve H_0 and σ_8 tensions?, *Eur. Phys. J. C* **81**, 482 (2021), [arXiv:2008.03966 \[astro-ph.CO\]](#).
- [52] N. Schöneberg, G. Franco Abellán, A. Pérez Sánchez, S. J. Witte, V. Poulin, and J. Lesgourgues, The H_0 Olympics: A fair ranking of proposed models, *Phys. Rept.* **984**, 1 (2022), [arXiv:2107.10291 \[astro-ph.CO\]](#).
- [53] J. Hubert, A. Schneider, D. Potter, J. Stadel, and S. K. Giri, Decaying dark matter: simulations and weak-lensing forecast, *JCAP* (10), 040, [arXiv:2104.07675 \[astro-ph.CO\]](#).
- [54] A. A. Sen, S. A. Adil, and S. Sen, Do cosmological observations allow a negative Λ ?, *Mon. Not. Roy. Astron. Soc.* **518**, 1098 (2022), [arXiv:2112.10641 \[astro-ph.CO\]](#).

- [55] D. K. Hazra, A. Antony, and A. Shafieloo, One spectrum to cure them all: signature from early Universe solves major anomalies and tensions in cosmology, *JCAP* **08** (08), 063, [arXiv:2201.12000 \[astro-ph.CO\]](#).
- [56] M. Kamionkowski and A. G. Riess, The Hubble Tension and Early Dark Energy, *Ann. Rev. Nucl. Part. Sci.* **73**, 153 (2023), [arXiv:2211.04492 \[astro-ph.CO\]](#).
- [57] J. Bucko, S. K. Giri, and A. Schneider, Constraining dark matter decay with cosmic microwave background and weak-lensing shear observations, *Astron. Astrophys.* **672**, A157 (2023), [arXiv:2211.14334 \[astro-ph.CO\]](#).
- [58] A. Gómez-Valent, A. Favale, M. Migliaccio, and A. A. Sen, Late-time phenomenology required to solve the H0 tension in view of the cosmic ladders and the anisotropic and angular BAO datasets, *Phys. Rev. D* **109**, 023525 (2024), [arXiv:2309.07795 \[astro-ph.CO\]](#).
- [59] S. A. Adil, Ö. Akarsu, E. Di Valentino, R. C. Nunes, E. Özülker, A. A. Sen, and E. Specogna, Omnipotent dark energy: A phenomenological answer to the Hubble tension, *Phys. Rev. D* **109**, 023527 (2024), [arXiv:2306.08046 \[astro-ph.CO\]](#).
- [60] Y. Tiwari, B. Ghosh, and R. K. Jain, Towards a possible solution to the Hubble tension with Horndeski gravity, *Eur. Phys. J. C* **84**, 220 (2024), [arXiv:2301.09382 \[astro-ph.CO\]](#).
- [61] V. Poulin, T. L. Smith, and T. Karwal, The Ups and Downs of Early Dark Energy solutions to the Hubble tension: A review of models, hints and constraints circa 2023, *Phys. Dark Univ.* **42**, 101348 (2023), [arXiv:2302.09032 \[astro-ph.CO\]](#).
- [62] G. Efstathiou, E. Rosenberg, and V. Poulin, Improved Planck Constraints on Axionlike Early Dark Energy as a Resolution of the Hubble Tension, *Phys. Rev. Lett.* **132**, 221002 (2024), [arXiv:2311.00524 \[astro-ph.CO\]](#).
- [63] O. Seto and Y. Toda, DESI constraints on the varying electron mass model and axionlike early dark energy, *Phys. Rev. D* **110**, 083501 (2024), [arXiv:2405.11869 \[astro-ph.CO\]](#).
- [64] V. Poulin, T. L. Smith, R. Calderón, and T. Simon, Implications of the cosmic calibration tension beyond H0 and the synergy between early- and late-time new physics, *Phys. Rev. D* **111**, 083552 (2025), [arXiv:2407.18292 \[astro-ph.CO\]](#).
- [65] Y. Toda, W. Giarè, E. Özülker, E. Di Valentino, and S. Vagnozzi, Combining pre- and post-recombination new physics to address cosmological tensions: Case study with varying electron mass and sign-switching cosmological constant, *Phys. Dark Univ.* **46**, 101676 (2024), [arXiv:2407.01173 \[astro-ph.CO\]](#).

- [66] E. Di Valentino *et al.* (CosmoVerse Network), The CosmoVerse White Paper: Addressing observational tensions in cosmology with systematics and fundamental physics, [Phys. Dark Univ.](#) **49**, 101965 (2025), [arXiv:2504.01669 \[astro-ph.CO\]](#).
- [67] E. M. Teixeira, W. Giarè, N. B. Hogg, T. Montandon, A. Poudou, and V. Poulin, Implications of distance duality violation for the H0 tension and evolving dark energy, [Phys. Rev. D](#) **112**, 023515 (2025), [arXiv:2504.10464 \[astro-ph.CO\]](#).
- [68] P. Mukherjee, D. Kumar, and A. A. Sen, Quintessential implications of the presence of AdS in the dark energy sector, [Phys. Rev. D](#) **113**, 063523 (2026), [arXiv:2501.18335 \[astro-ph.CO\]](#).
- [69] H. Cheng, E. Di Valentino, L. A. Escamilla, A. A. Sen, and L. Visinelli, Pressure parametrization of dark energy: first and second-order constraints with latest cosmological data, [JCAP](#) (09), 031, [arXiv:2505.02932 \[astro-ph.CO\]](#).
- [70] R. Shah, P. Mukherjee, and S. Pal, Interacting dark sectors in light of DESI DR2, [Mon. Not. Roy. Astron. Soc.](#) **542**, 2936 (2025), [arXiv:2503.21652 \[astro-ph.CO\]](#).
- [71] E. Mortsell, A. Goobar, J. Johansson, and S. Dhawan, Sensitivity of the Hubble Constant Determination to Cepheid Calibration, [Astrophys. J.](#) **933**, 212 (2022), [arXiv:2105.11461 \[astro-ph.CO\]](#).
- [72] E. Mortsell, A. Goobar, J. Johansson, and S. Dhawan, The Hubble Tension Revisited: Additional Local Distance Ladder Uncertainties, [Astrophys. J.](#) **935**, 58 (2022), [arXiv:2106.09400 \[astro-ph.CO\]](#).
- [73] W. L. Freedman, Measurements of the Hubble Constant: Tensions in Perspective, [Astrophys. J.](#) **919**, 16 (2021), [arXiv:2106.15656 \[astro-ph.CO\]](#).
- [74] K. Jedamzik, L. Pogosian, and G.-B. Zhao, Why reducing the cosmic sound horizon alone can not fully resolve the Hubble tension, [Commun. in Phys.](#) **4**, 123 (2021), [arXiv:2010.04158 \[astro-ph.CO\]](#).
- [75] J. Evslin, A. A. Sen, and Ruchika, Price of shifting the Hubble constant, [Phys. Rev. D](#) **97**, 103511 (2018), [arXiv:1711.01051 \[astro-ph.CO\]](#).
- [76] M. Chevallier and D. Polarski, Accelerating universes with scaling dark matter, [Int. J. Mod. Phys. D](#) **10**, 213 (2001).
- [77] E. V. Linder, Exploring the expansion history of the universe, [Phys. Rev. Lett.](#) **90**, 091301 (2003).

- [78] Z. Berezhiani, A. D. Dolgov, and I. I. Tkachev, Reconciling Planck results with low redshift astronomical measurements, *Phys. Rev. D* **92**, 061303 (2015), [arXiv:1505.03644 \[astro-ph.CO\]](#).
- [79] A. Chudaykin, D. Gorbunov, and I. Tkachev, A dark matter component decaying after recombination: lensing constraints with Planck data, *EPJ Web Conf.* **125**, 03004 (2016).
- [80] L. Xiao, L. Zhang, R. An, C. Feng, and B. Wang, Fractional Dark Matter decay: cosmological imprints and observational constraints, *JCAP* (01), 045, [arXiv:1908.02668 \[astro-ph.CO\]](#).
- [81] A. Nygaard, T. Tram, and S. Hannestad, Updated constraints on decaying cold dark matter, *JCAP* (05), 017, [arXiv:2011.01632 \[astro-ph.CO\]](#).
- [82] N. Blinov, C. Keith, and D. Hooper, Warm Decaying Dark Matter and the Hubble Tension, *JCAP* (06), 005, [arXiv:2004.06114 \[astro-ph.CO\]](#).
- [83] G. Franco Abellán, R. Murgia, and V. Poulin, Linear cosmological constraints on two-body decaying dark matter scenarios and the S8 tension, *Phys. Rev. D* **104**, 123533 (2021), [arXiv:2102.12498 \[astro-ph.CO\]](#).
- [84] E. B. Holm, T. Tram, and S. Hannestad, Decaying warm dark matter revisited, *JCAP* **08** (08), 044, [arXiv:2205.13628 \[astro-ph.CO\]](#).
- [85] S. Alvi, T. Brinckmann, M. Gerbino, M. Lattanzi, and L. Pagano, Do you smell something decaying? Updated linear constraints on decaying dark matter scenarios, *JCAP* (11), 015, [arXiv:2205.05636 \[astro-ph.CO\]](#).
- [86] L. A. Anchordoqui, V. Barger, D. Marfatia, and J. F. Soriano, Decay of multiple dark matter particles to dark radiation in different epochs does not alleviate the Hubble tension, *Phys. Rev. D* **105**, 103512 (2022), [arXiv:2203.04818 \[astro-ph.CO\]](#).
- [87] Z. Davari and N. Khosravi, Can decaying dark matter scenarios alleviate both H_0 and σ_8 tensions?, *Mon. Not. Roy. Astron. Soc.* **516**, 4373 (2022), [arXiv:2203.09439 \[astro-ph.CO\]](#).
- [88] T. Simon, G. Franco Abellán, P. Du, V. Poulin, and Y. Tsai, Constraining decaying dark matter with BOSS data and the effective field theory of large-scale structures, *Phys. Rev. D* **106**, 023516 (2022), [arXiv:2203.07440 \[astro-ph.CO\]](#).
- [89] T. Simon, Constraining decaying dark matter with the effective field theory of large-scale structure, in *33rd Rencontres de Blois: Exploring the Dark Universe* (2022) [arXiv:2212.03004 \[astro-ph.CO\]](#).
- [90] G. Gambini, P. C. de Holanda, and S. Carneiro, Constraints on Energy Scales from Dark Matter Decay in a Gauged $B - L$ Model, *Braz. J. Phys.* **56**, 30 (2026), [arXiv:2205.12353](#)

[hep-ph].

- [91] J. Bucko, S. K. Giri, F. H. Peters, and A. Schneider, Probing the two-body decaying dark matter scenario with weak lensing and the cosmic microwave background, *Astron. Astrophys.* **683**, A152 (2024), [arXiv:2307.03222 \[astro-ph.CO\]](#).
- [92] Q. Zhou, Z. Xu, and S. Zheng, Interpreting Hubble tension with a cascade decaying dark matter sector, - (2025), [arXiv:2507.08687 \[astro-ph.CO\]](#).
- [93] J. Juárez-Jiménez and A. A. Avilez-López, Forecasts for lifetime and fraction of Decaying Dark Matter based on redshift distortions from Euclid and BOSS, - (2025), [arXiv:2512.03348 \[astro-ph.CO\]](#).
- [94] R. J. Scherrer, Mapping the Chevallier-Polarski-Linder parametrization onto Physical Dark Energy Models, *Phys. Rev. D* **92**, 043001 (2015), [arXiv:1505.05781 \[astro-ph.CO\]](#).
- [95] S. Tsujikawa, Quintessence: A Review, *Class. Quant. Grav.* **30**, 214003 (2013), [arXiv:1304.1961 \[gr-qc\]](#).
- [96] S. Vagnozzi, Seven Hints That Early-Time New Physics Alone Is Not Sufficient to Solve the Hubble Tension, *Universe* **9**, 393 (2023), [arXiv:2308.16628 \[astro-ph.CO\]](#).
- [97] M. Abdul Karim *et al.* (DESI), DESI DR2 results. II. Measurements of baryon acoustic oscillations and cosmological constraints, *Phys. Rev. D* **112**, 083515 (2025), [arXiv:2503.14738 \[astro-ph.CO\]](#).
- [98] D. Brout *et al.*, The Pantheon+ Analysis: Cosmological Constraints, *Astrophys. J.* **938**, 110 (2022), [arXiv:2202.04077 \[astro-ph.CO\]](#).
- [99] V. Poulin, P. D. Serpico, and J. Lesgourgues, A fresh look at linear cosmological constraints on a decaying dark matter component, *JCAP* (08), 036, [arXiv:1606.02073 \[astro-ph.CO\]](#).
- [100] B. Audren, J. Lesgourgues, G. Mangano, P. D. Serpico, and T. Tram, Strongest model-independent bound on the lifetime of Dark Matter, *JCAP* **12** (-), 028, [arXiv:1407.2418 \[astro-ph.CO\]](#).
- [101] É. Aubourg *et al.* (BOSS), Cosmological implications of baryon acoustic oscillation measurements, *Phys. Rev. D* **92**, 123516 (2015), [arXiv:1411.1074 \[astro-ph.CO\]](#).
- [102] C.-P. Ma and E. Bertschinger, Cosmological perturbation theory in the synchronous and conformal Newtonian gauges, *Astrophys. J.* **455**, 7 (1995), [arXiv:astro-ph/9506072](#).
- [103] A. G. Riess *et al.* (Supernova Search Team), Observational evidence from supernovae for an accelerating universe and a cosmological constant, *Astron. J.* **116**, 1009 (1998), [arXiv:astro-](#)

- ph/9805201.
- [104] S. Weinberg, The cosmological constant problem, *Rev. Mod. Phys.* **61**, 1 (1989).
- [105] S. M. Carroll, The Cosmological constant, *Living Rev. Rel.* **4**, 1 (2001), [arXiv:astro-ph/0004075](#).
- [106] P. J. E. Peebles and B. Ratra, The Cosmological Constant and Dark Energy, *Rev. Mod. Phys.* **75**, 559 (2003), [arXiv:astro-ph/0207347](#).
- [107] B. Ratra and P. J. E. Peebles, Cosmological consequences of a rolling homogeneous scalar field, *Phys. Rev. D* **37**, 3406 (1988).
- [108] R. R. Caldwell, R. Dave, and P. J. Steinhardt, Cosmological imprint of an energy component with general equation of state, *Phys. Rev. Lett.* **80**, 1582 (1998).
- [109] I. Zlatev, L. Wang, and P. J. Steinhardt, Quintessence, cosmic coincidence, and the cosmological constant, *Phys. Rev. Lett.* **82**, 896 (1999).
- [110] R. R. Caldwell, A Phantom menace?, *Phys. Lett. B* **545**, 23 (2002), [arXiv:astro-ph/9908168](#).
- [111] H. Stefancic, Dark energy transition between quintessence and phantom regimes - An Equation of state analysis, *Phys. Rev. D* **71**, 124036 (2005), [arXiv:astro-ph/0504518](#).
- [112] E. J. Copeland, M. Sami, and S. Tsujikawa, Dynamics of dark energy, *Int. J. Mod. Phys. D* **15**, 1753 (2006), [arXiv:hep-th/0603057](#).
- [113] P. Creminelli, G. D'Amico, J. Norena, and F. Vernizzi, The Effective Theory of Quintessence: the $w < -1$ Side Unveiled, *JCAP* (2), 18, [arXiv:0811.0827 \[astro-ph\]](#).
- [114] T. Louis *et al.* (Atacama Cosmology Telescope), The Atacama Cosmology Telescope: DR6 power spectra, likelihoods and Λ CDM parameters, *JCAP* (11), 062, [arXiv:2503.14452 \[astro-ph.CO\]](#).
- [115] J. Torrado and A. Lewis, Cobaya: Code for Bayesian Analysis of hierarchical physical models, *JCAP* (05), 057, [arXiv:2005.05290 \[astro-ph.IM\]](#).
- [116] D. Blas, J. Lesgourgues, and T. Tram, The cosmic linear anisotropy solving system (class). part ii: Approximation schemes, *Journal of Cosmology and Astroparticle Physics* **2011** (07), 034.
- [117] A. Gelman and D. B. Rubin, Inference from Iterative Simulation Using Multiple Sequences, *Statistical Science* **7**, 457 (1992).
- [118] R. Trotta, Bayes in the sky: Bayesian inference and model selection in cosmology, *Contemp. Phys.* **49**, 71 (2008), [arXiv:0803.4089 \[astro-ph\]](#).

- [119] G. Mangano and P. D. Serpico, A robust upper limit on n_{eff} from bbn, circa 2011, *Physics Letters B* **701**, 296 (2011).
- [120] R. H. Cyburt, B. D. Fields, K. A. Olive, and T.-H. Yeh, Big Bang Nucleosynthesis: 2015, *Rev. Mod. Phys.* **88**, 015004 (2016), [arXiv:1505.01076 \[astro-ph.CO\]](#).
- [121] F.-Y. Cyr-Racine, R. de Putter, A. Raccanelli, and K. Sigurdson, Constraints on Large-Scale Dark Acoustic Oscillations from Cosmology, *Phys. Rev. D* **89**, 063517 (2014), [arXiv:1310.3278 \[astro-ph.CO\]](#).
- [122] M. Garny, F. Niedermann, H. Rubira, and M. S. Sloth, Hot New Early Dark Energy: Dark Radiation Matter Decoupling, - (2025), [arXiv:2508.03795 \[astro-ph.CO\]](#).
- [123] M. Garny, F. Niedermann, and M. S. Sloth, Dark Acoustic Oscillations as an Early-Universe Explanation of the DESI Anomaly, - (2025), [arXiv:2512.15870 \[astro-ph.CO\]](#).
- [124] W. Elbers *et al.*, Constraints on neutrino physics from DESI DR2 BAO and DR1 full shape, *Phys. Rev. D* **112**, 083513 (2025), [arXiv:2503.14744 \[astro-ph.CO\]](#).
- [125] H. Shao, J. J. Givans, J. Dunkley, M. Madhavacheril, F. J. Qu, G. Farren, and B. Sherwin, Cosmological limits on the neutrino mass sum for beyond- Λ CDM models, *Phys. Rev. D* **111**, 083535 (2025), [arXiv:2409.02295 \[astro-ph.CO\]](#).
- [126] W. J. Handley, M. P. Hobson, and A. N. Lasenby, PolyChord: nested sampling for cosmology, *Mon. Not. Roy. Astron. Soc.* **450**, L61 (2015), [arXiv:1502.01856 \[astro-ph.CO\]](#).
- [127] A. He, M. M. Ivanov, R. An, and V. Gluscevic, S_8 Tension in the Context of Dark Matter–Baryon Scattering, *Astrophys. J. Lett.* **954**, L8 (2023), [arXiv:2301.08260 \[astro-ph.CO\]](#).
- [128] R. Dhyani, A. Paul, and A. Chatterjee, Probing Dark Matter-electron interactions in the Cosmic Microwave Background Radiation, *JCAP* (10), 046, [arXiv:2503.04539 \[hep-ph\]](#).
- [129] V. Poulin, T. L. Smith, R. Calderón, and T. Simon, Impact of ACT DR6 and DESI DR2 for early dark energy and the Hubble tension, *Phys. Rev. D* **113**, 063519 (2026), [arXiv:2505.08051 \[astro-ph.CO\]](#).
- [130] M. Bella, V. Poulin, S. Vagnozzi, and L. Knox, Double the axions, half the tension: multi-field early dark energy eases the Hubble tension, - (2026), [arXiv:2604.13535 \[astro-ph.CO\]](#).
- [131] T. Jhaveri, T. Karwal, T. Crawford, W. Hu, A. R. Khalife, L. Balkenhol, and F. Ge, Disentangling cosmic distance tensions with early and late dark energy, - (2026), [arXiv:2604.08530 \[astro-ph.CO\]](#).

- [132] J. Lesgourgues *et al.* (Euclid), Euclid preparation - LVI. Sensitivity to non-standard particle dark matter models, *Astron. Astrophys.* **693**, A249 (2025), [arXiv:2406.18274 \[astro-ph.CO\]](#).
- [133] N. E. Chisari *et al.* (LSST Dark Energy Science), Core Cosmology Library: Precision Cosmological Predictions for LSST, *Astrophys. J. Suppl.* **242**, 2 (2019), [arXiv:1812.05995 \[astro-ph.CO\]](#).